A Supramolecular Helix that Disregards Chirality

Cécile Roche,[†] Hao-Jan Sun,[†,‡] Pawaret Leowanawat,[†] Fumito Araoka,[≠] Benjamin E. Partridge,[†] Mihai Peterca,[†] Daniela A. Wilson,[†] Margaret E. Prendergast,[†] Paul A. Heiney,[‡] Robert Graf,[§] Hans W. Spiess,[§] Xiangbing Zeng,[¶] Goran Ungar,[¶,♣] and Virgil Percec*[,†]

[†]Roy & Diana Vagelos Laboratories, Department of Chemistry, University of Pennsylvania, Philadelphia, Pennsylvania 19104-6323, United States. [‡]Department of Physics and Astronomy, University of Pennsylvania, Philadelphia, Pennsylvania 19104-6396, United States. [≠]RIKEN Center for Emergent Matter Science (CEMS), 2-1 Hirosawa, Wako, Saitama 351-0198, Japan. [§]Max-Planck Institute for Polymer Research, 55128 Mainz, Germany. [¶]Department of Materials Science and Engineering, University of Sheffield, Sheffield S1 3JD, United Kingdom. [♣]Department of Physics, Zhejiang Sci-Tech University, Hangzhou 310018, China

Functions of complex crystalline systems derived from natural and synthetic macromolecules emerge from homochiral programmed primary structures via first principles involving secondary, tertiary and quaternary structures. Heterochiral and racemic compounds yield disordered crystals, amorphous solids or liquids. Supramolecular biological and nonbiological assemblies follow the same principles. Here we report the self-organization of a supramolecular helix that forms columnar hexagonal crystals with similar precision to biological systems. This high crystalline order is generated via a cogwheel mechanism that disregards the chirality of the self-assembling building blocks. We show that both homochiral and racemic compounds, including a mixture of 21 diastereomers that cannot be deracemized at the molecular level, self-organize to form single-handed helical assemblies with identical single crystal-like order. We anticipate that this new mechanism will facilitate access to previously inaccessible complex crystalline systems from racemic and homochiral building blocks.

The origin of biological homochirality remains a fundamental question of natural science,[1–5] even though the most advanced functions of biological and nonbiological systems emerge from homochiral primary structures. Classic examples are the helical structure of proteins,[6] carbohydrates,[7] isotactic polypropylene,[8,9] carbon nanotubes[10–12] and the double helix of DNA.[13–15] These secondary structures, together with other local conformations, are responsible for the creation of tertiary and quaternary crystalline structures[15,16] and functions. Heterochiral primary structures such as syndiotactic polypropylene[8,17] yield lower order crystals than their homochiral counterparts while racemic or atactic polymers generate amorphous solids or liquids.[8] Since Pasteur's seminal experiment,[18] chiral self-sorting, or spontaneous deracemization, of conglomerates during crystallization from solution[18–25] has been employed to generate homochirality at the single crystal

scale but not at the macroscopic level. This was demonstrated by conglomerates having lower melting points than crystals of the corresponding pure enantiomers.[21] Spontaneous deracemization of helical assemblies produced from achiral molecules in thermotropic liquid crystals translated deracemization from solution[18–25] to bulk liquid crystal state.[26–28] This advance enabled access to monodomains of enantiomerically pure liquid crystals by spontaneous deracemization in melt liquid crystal states.[26–28] The same homochiral principles have been demonstrated during self-organization of supramolecular biological assemblies, such as tobacco mosaic virus,[29,30] and non-biological assemblies.[31–41] A study of all stereochemical permutations of self-assembling dendritic dipeptides, including homochiral, heterochiral and various racemic variants in solution and bulk state, demonstrated that the highest degree of stereochemical purity, enantiopure homochiral, exhibited the most thermodynamically favored self-assembly process in solution, corresponding to the greatest degree of order in the crystal state.[31–34] These results showed that enantiomerically rich, racemic and achiral assemblies may undergo deracemization even in sufficiently mobile crystal states, when the transfer of a molecule between neighboring assemblies is thermodynamically and kinetically allowed. Supramolecular assemblies of dendritic dipeptides held together via strong noncovalent interactions approaching the strength of a covalent bond precluded deracemization due to prohibited disassembly.[32] Therefore, their homochiral assemblies could crystallize while their racemic assemblies could not.[32] A recent study of the self-assembly of a family of weakly interacting, dynamic cyclotriveratrylene crowns substituted with 12 branched alkyl chains of various chiral compositions demonstrated the first example of deracemization in the crystalline state.[21] The driving force for deracemization was formation of a columnar hexagonal crystal, whose lattice symmetry demands identical single-handed helical columns in a crystal lattice whose unit cell contains fragments of four separate columns representing a single column.[21] This was possible due to the weak supramolecular interactions between crowns. Homochiral and "racemic by mixture" samples were shown to deracemize at the molecular level to generate crystalline order after annealing. However, a "racemic by synthesis" sample, which intrinsically cannot deracemize at the molecular level, was unable to generate high crystalline order and instead yielded poorly ordered columnar hexagonal crystals upon deracemization, with a much lower melting temperature than the corresponding enantiopure forms.[21] This study also demonstrated that deracemization at the supramolecular level occurs between enantiomerically pure or enantiomerically rich supramolecular columns rather than within a column.

Here we report the discovery of a family of perylene bisimide (PBI) derivatives containing six chiral side chains in various stereochemical permutations including homochiral, "racemic by mixing" and "racemic by synthesis" that self-assembles into single-handed supramolecular columns to yield identical single-handed columnar hexagonal crystalline domains likely due to deracemization at the molecular and supramolecular

levels, irrespective of chiral composition. A cogwheel model of crystallization was proposed to facilitate this process and to explain the very high degree of order even at the interface between single-handed crystalline monodomains. A library of chiral PBI derivatives was screened in order to discover the compounds reported here. This cogwheel mechanism responsible for the generation of single crystal-like order from racemic compounds is expected to enable prediction of libraries of building blocks that follow the same self-organization principles, via the design of other self-assembling molecules with structural parameters congruent with the present PBI derivatives.

Results and Discussion

Synthesis of building blocks and their self-organization in bulk. The synthesis of four PBI derivatives substituted with two identical benzyl rings bearing three chiral dimethyloctyloxy chains in either enantiopure (**(R)-11** and **(S)-11**) or racemic form (**rac-11** and **mix-11**) is outlined in Fig. 1a. The two helical models of the supramolecular columns formed by **11** are shown in Fig. 1b, c (Supporting Sections S19 and S20). An overview of previously reported helical assemblies of PBI is in Supplementary Section S4.

The length of the dimethyloctyl chains and the alkyl spacer between PBI and benzyl ring were selected to achieve a thermodynamically controlled crystallization of their assemblies as discovered previously with linear achiral alkyloxy groups.[42] **(S)-8** and **(R)-8** are enantiomerically pure, whereas the racemic **rac-8** is a mixture of 6 diastereomers with different chiralities of the side chains at the 3-, 4- and 5-positions of the benzyl ring. Consequently, **(S)-11** and **(R)-11** are enantiomerically pure, while **rac-11**, named also "racemic by synthesis", contains 21 diastereomers whose chirality is statistically scrambled. **rac-11** differs from "racemic by mixing" **mix-11**, which is a 50:50 mixture of the homochiral enantiomers **(S)-11** and **(R)-11**.

Differential scanning calorimetry (DSC) (Supplementary Fig. S2) combined with X-ray diffraction (XRD) experiments (to be discussed later) demonstrated unexpected behavior of the assemblies obtained from the enantiopure (**(S)-11**, **(R)-11**) and racemic (**rac-11**, **mix-11**) compounds. All assemblies exhibit a columnar hexagonal crystalline phase, $\mathbf{\Phi_h^{k1}}$, formed under thermodynamic control,[42] which melts at 200 °C with almost no hysteresis; it crystallizes at 198 °C and 199 °C with cooling rates of 10 °C/min and 1 °C/min, respectively. Low order $\mathbf{\Phi_h^{k1}}$ is metastable at low temperature; high order $\mathbf{\Phi_h^{k2}}$, formed under kinetic control, can be detected only by special thermal treatment such as (i) slow heating and reheating (1 °C/min) via an exotherm at ~105 °C observed upon heating (Supplementary Figs S2 and S10), (ii) rapid heating (10 °C/min) followed by annealing at 110 °C for 3 h (Supplementary Fig. S2) or (iii) an extended period of annealing at 23 °C (Supplementary Fig. S12). Upon heating, $\mathbf{\Phi_h^{k2}}$ transforms into $\mathbf{\Phi_h^{k1}}$ at 128–130 °C.

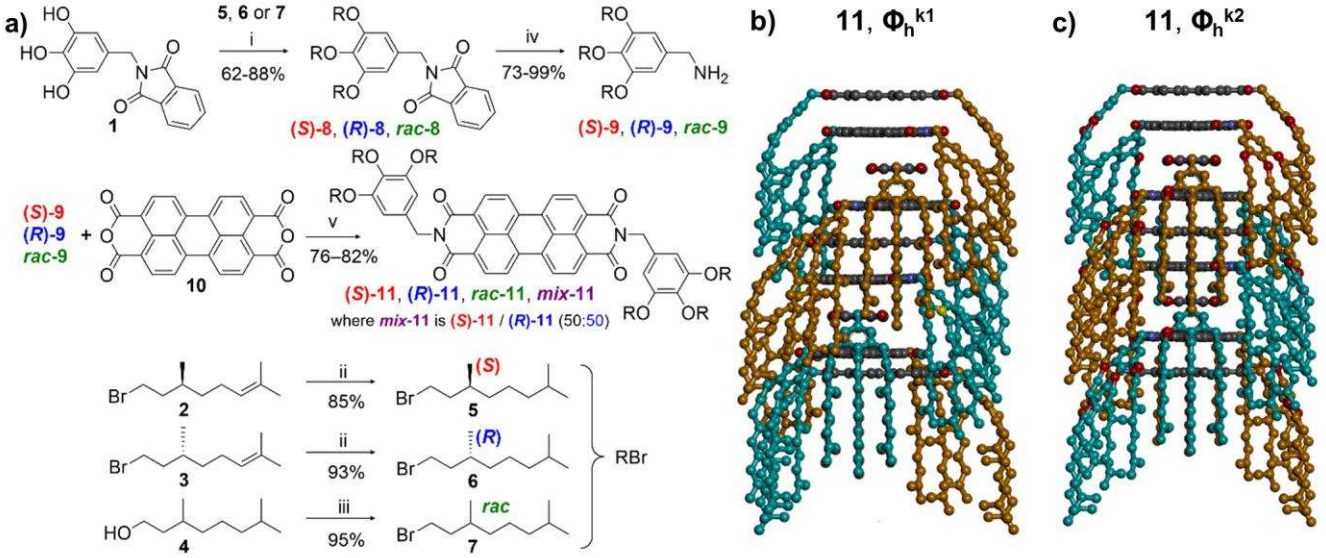

Figure 1. Synthesis and supramolecular structure of PBI derivatives. a, Synthesis of chiral PBI derivatives **(S)-11** and **(R)-11**, "racemic by synthesis" **(rac)-11**, which is a statistical mixture of all possible diastereomers synthesized from racemic bromide **7**, and "racemic by mixing" **(mix)-11**, which is a 50:50 mixture of the two enantiomers **(S)-11** and **(R)-11**. Reagents and conditions: (i) K_2CO_3, DMF, 70 °C; (ii) H_2, PtO_2, EtOAc, 25 °C; (iii) HBr, H_2SO_4 (cat.), 120 °C; (iv) $NH_2NH_2 \cdot H_2O$, graphite, EtOH, reflux; (v) $Zn(OAc)_2 \cdot 2H_2O$, quinoline, 180 °C. **b**, **c**, Comparison of the helical structures of **b**, **11** in the low order $\mathbf{\Phi_h^{k1}}$ phase and **c**, **11** in the high order $\mathbf{\Phi_h^{k2}}$ phase. The supramolecular helix in the low order $\mathbf{\Phi_h^{k1}}$ phase is slightly distorted, resulting in a wavy surface on the exterior of the supramolecular column. In contrast, the supramolecular columns in the high order $\mathbf{\Phi_h^{k2}}$ phase are crystallographically perfect helices with a straight surface along the length of the column.

Analysis of self-assembly in solution by CD and UV-vis. Circular dichroism (CD) and UV-vis spectra of solutions of **(S)-11** and **(R)-11** in n-butanol/methylcyclohexane (85:15 v/v) recorded upon cooling from 50 °C to 10 °C demonstrate that self-assembly of **11** proceeds via two distinct stages (Fig. 2a). In the first stage, from 50 °C to 20 °C, **(S)-11** and **(R)-11** are CD-silent. However, a significant decrease in the intensity of their UV-vis absorbance is observed. This suggests that **(S)-11** and **(R)-11** are molecularly dissolved at 50 °C and form short disordered stacks, such as dimers or trimers, upon cooling to 20 °C. The absence of Cotton effects between 50 °C and 20 °C excludes the formation of long, ordered helical assemblies. In the second stage, from 20 °C to 10 °C, an intense Cotton effect emerges in the CD spectra, evidencing the formation of an extended helical assembly (Fig. 2a, top). The spectra of **(S)-11** are mirror images of those of **(R)-11**, confirming that the chirality of the peripheral alkyl chains selects the handedness of the helical assemblies. The intense Cotton effects in the visible region confirm the transfer and amplification of chirality from the dimethyloctyl chains to the aromatic core of the assembly. The positive exciton coupling of **(R)-11** implies formation of a right-handed helix, while the negative exciton coupling of **(S)-11** indicates a left-handed helix (Supplementary Section S7). The first stage of self-assembly, from 50 °C to 20 °C, observed only by UV-vis but not by CD, is associated with a nucleation process, while the

second part, from 20 °C to 10 °C, active in both CD and UV-vis, is associated with growth of the helix via a supramolecular helical polymerization mechanism.[21,30,43–45] CD experiments in thin film and in solution (solid and broken lines, respectively, in Fig. 2b) indicate persistence of a similar helical structure in both states.

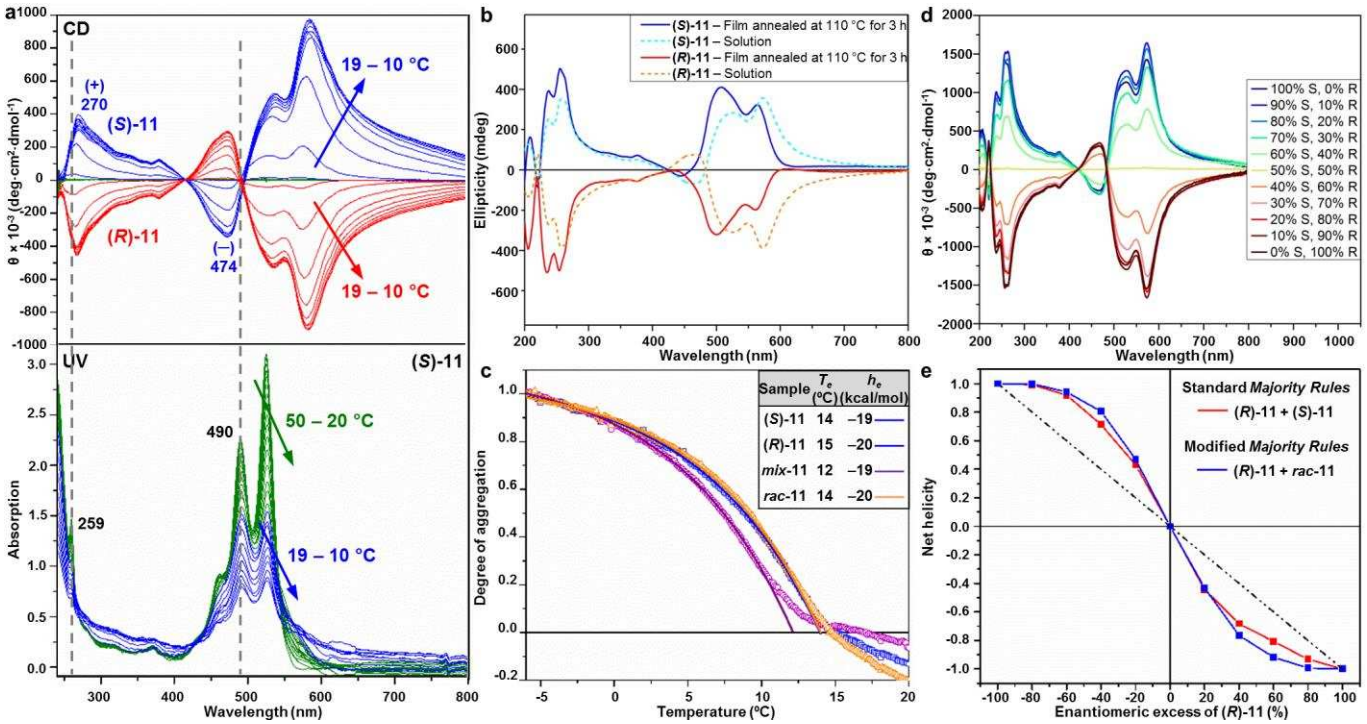

Figure 2. Solution CD and UV-vis experiments. a, Solution CD and UV-vis spectra of **(S)-11** and **(R)-11** upon cooling. **(S)-11**: green (50 to 20 °C) and blue (19 to 10 °C); **(R)-11**: red (19 to 10 °C). UV spectra for **(R)-11** and **(S)-11** are identical. **b**, CD spectra of thin films (solid lines) of **(S)-11** (blue) and **(R)-11** (red) (collected at 23 °C). Solution spectra are also given (broken lines). **c**, Degree of aggregation of **(S)-11** (blue), **(R)-11** omitted for clarity, **mix-11** (purple), and **rac-11** (orange) calculated from UV-vis data upon cooling, and fitting with the cooperative elongation model (solid lines). Calculated[46] values for the elongation enthalpy, h_e and elongation temperature, T_e are tabulated in the inset. **d**, **e**, Majority rules experiments; **d**, CD spectra collected from mixtures of **(R)-11** and **(S)-11**. **e**, Net helicity dependence on the enantiomeric excess in mixtures of **(R)-11** and **(S)-11** (red) and **(R)-** or **(S)-11** and **rac-11** (blue). These experiments demonstrate not only that **(R)-11** and **(S)-11** generate supramolecular assemblies of opposite handedness in solution, but also that these structures show some disregard for chirality during self-assembly in solution.

Variable temperature CD/UV-vis experiments in solution performed on all variants of **11** demonstrate a cooperative nucleation mechanism for their helical supramolecular polymerization (Fig. 2c).[21,30,32,34,43–45] Quantitative thermodynamic analysis from UV-vis data demonstrated, within experimental error, identical values for the elongation enthalpy, h_e, and elongation temperature, T_e, irrespective of enantiomeric composition (inset, Fig. 2c). The elongation enthalpy, h_e, represents the net enthalpy change upon elongation of the supramolecular column, while the elongation temperature, T_e, represents the temperature

at which the nucleating assemblies begin to elongate to form extended helical segments.[46] The slightly lower T_e of **mix-11** may be due to heterogeneous nucleation mediated by the mismatched enantiomer impurity acting as a seed.[32] The negative sign of h_e confirms that self-assembly is enthalpically driven. These results agree with X-ray data (to be discussed later), which reveal identical structures in all cases and suggest that the enthalpic energy gained by addition of a PBI molecule to the supramolecular structure is almost invariant to the chirality of the molecule being added. In other words, addition of a matching or a mismatching monomer to a helical column are similarly favorable and the calculated enthalpy is an average value. The elongation enthalpy, h_e, should reflect the non-zero mismatch penalty (0.6 kcal/mol; Supplementary Table S2) but experimental uncertainty in the value of h_e (±1 kcal/mol) obscures its influence. Therefore, in contrast to previous studies,[21] h_e shows that the thermodynamic stability and the supramolecular structure of homochiral and racemic compounds do not strongly depend, at least in solution, on the enantiomeric purity of their side chains.

Majority rules experiments probe whether a system exhibits chiral amplification.[21,24,32–34,47–49] In a system with no chiral amplification, the net ellipticity of a mixture of two enantiomers changes linearly with enantiomeric excess (Fig. 2e, broken black line). In contrast, a deviation from linearity suggests that the enantiomer in excess has a disproportionate impact upon the handedness of the supramolecular assemblies generated, as observed in majority rules experiments with **(R)-11** and **(S)-11** (Fig. 2e, red) and with **(R)-** or **(S)-11** and **rac-11** (Fig. 2e, blue). This moderate non-linear effect suggests that the enantiomers can co-assemble into a single column in solution and that the majority enantiomer dictates the helical sense of the column. The similarity of the deviation from linearity in both majority rules experiments suggests that elongation of a helical column with a monomer of the non-preferred chirality is only slightly less unfavorable for a monomer with all six stereocenters of the non-preferred chirality (i.e. **(R)-** or **(S)-11**) as it is for a monomer with as little as one stereocenter of the non-preferred chirality (**rac-11**). Hence a disregard for chirality is evident in the assembly of helical supramolecular columns in solution.

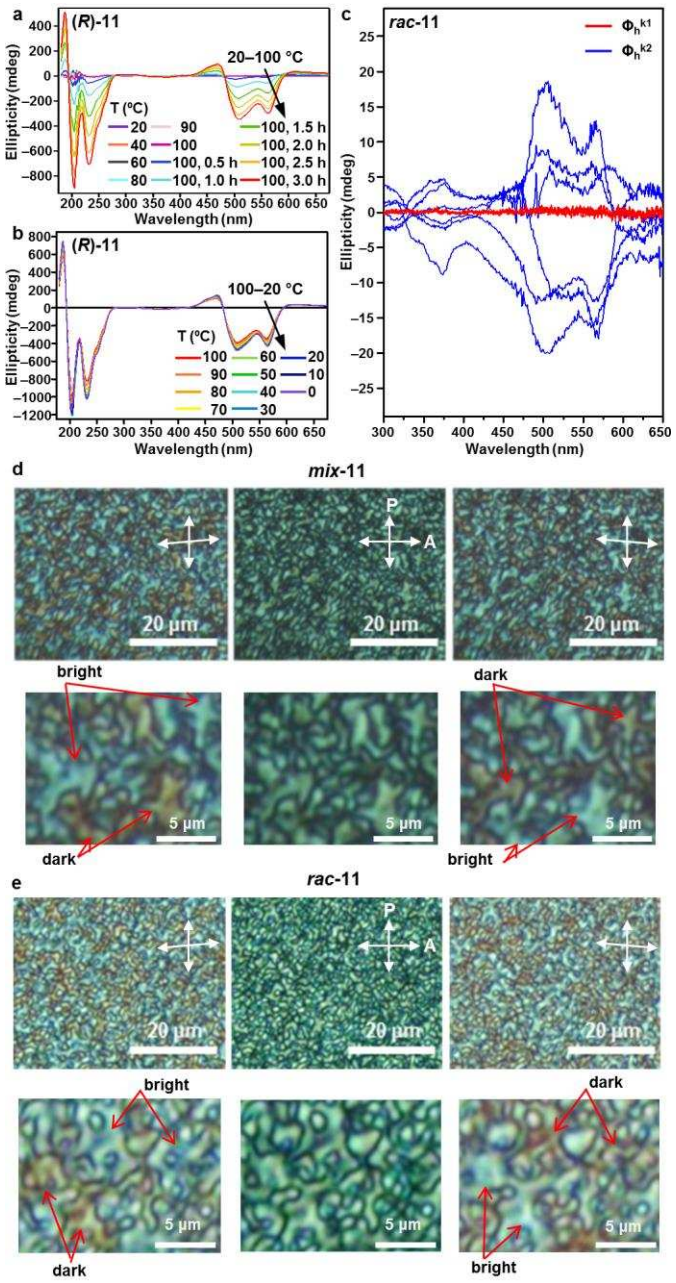

Figure 3. **Thin film CD and optical polarized microscopy studies. a**, **b**, Thin film CD spectra of **(R)-11** during **a**, heating from 20 to 100 °C followed by annealing at 100 °C and **b**, cooling from 100 °C after annealing. **c**, Thin film micro-spot CD spectra of **rac-11** in the (red) $\mathbf{\Phi_h^{k1}}$ and (blue) $\mathbf{\Phi_h^{k2}}$ phases. Each spectrum was obtained from a different spot on the film at 23 °C. Thin film micro-spot CD spectra of racemic by mixing **mix-11** and enantiopure **(S)-** and **(R)-11** are in Supplementary Figs S7 and S8. **d**, **e**, Optical polarized micrographs of **d**, **mix-11** and **e**, **rac-11** in the $\mathbf{\Phi_h^{k2}}$ phase, from the same films used for micro-spot CD. The analyzer was rotated ±5º from the crossed position in the right and left micrographs, respectively. Bright and dark areas (blue and brown, respectively) are indicated. The directions of polarizer (P) and analyzer (A) are ~~shown~~ denoted by arrows (top). The emergence of distinct positive and negative CD signals in a film of **rac-11** demonstrates segregation into microdomains of supramolecular columns of a single handedness. Optical polarized micrographs show these microdomains as distinct areas, the contrast of which changes from bright to dark, or vice versa, upon rotating an analyzer in different directions.

Analysis of the self-assembly in bulk by CD, micro-spot CD and optical polarized microscopy. The helicity of assemblies in Φ_h^{k1} and Φ_h^{k2} was investigated in a thin film of **(R)-11** monitored by CD during annealing (Fig. 3a, b). No Cotton effect was observed in the as prepared film at temperatures lower than 100 °C, indicating that assemblies in Φ_h^{k1} either have no well-defined handedness or exist as an equal mixture of right- and left-handed columns (Fig. 3a). Heating and annealing at 100 °C transformed Φ_h^{k1} into Φ_h^{k2} and the Cotton effect increased dramatically, demonstrating that assemblies in Φ_h^{k2} exhibit a well-defined helical structure that is stable upon cooling to 20 °C (Fig. 3b). Neither **rac-11** nor **mix-11** exhibit a CD signal in solution or in a thin film annealed under the same conditions as for **(R)-11**, suggesting that both racemic samples contain a mixture of either an equal number of helical columns with opposite handednesses (racemic between columns) or columns with a helix inversion and an equal amount of right- and left-handed helical segments (racemic within a column). Micro-spot CD experiments on films of **rac-11** (Fig. 3c) and **mix-11** (Supplementary Figure S7) in the Φ_h^{k1} and Φ_h^{k2} phases were performed to discriminate between these two possibilities.[21] The birefringence of these films was confirmed to be negligibly small (Supplementary Section S11), as also supported by thin film micro-spot CD spectra of enantiopure **(S)-** and **(R)-11** (Supplementary Fig. S8). Micro-spot CD experiments demonstrated that Φ_h^{k2} of **mix-11** (Supplementary Figure S7) and surprisingly also **rac-11** (Fig. 3c, blue) consists of domains containing columns of a single handedness. A control experiment on Φ_h^{k1} of **rac-11** (Fig. 3c, red) shows no deracemization in the low order Φ_h^{k1} phase. Therefore, deracemization takes place between left- and right-handed homochiral supramolecular columns in the crystal state, as demonstrated for the first time recently.[21] Optical segregation of enantiopure domains was also identified by uncrossing the polarizers of an optical polarized microscope. Enantiomeric domains are distinguished as bright and dark regions that interchange by rotating the analyzer clockwise or counterclockwise (Fig. 3d, e). These experiments support a chiral self-sorting or deracemization process[18,21] occurring for assemblies of **mix-11** and **rac-11** during the transition to the columnar hexagonal crystal phase, Φ_h^{k2}. A control experiment with homochiral **(S)-** and **(R)-11** (Supplementary Figure S9) shows no relative change in the contrast of individual microdomains, but rather an overall change across the entire film. This indicates the presence of microdomains of a single handedness throughout Φ_h^{k2}, as expected from homochiral samples. We conclude that in Φ_h^{k2} the supramolecular columns generated from all four homochiral and racemic compounds are single-handed and homochiral.

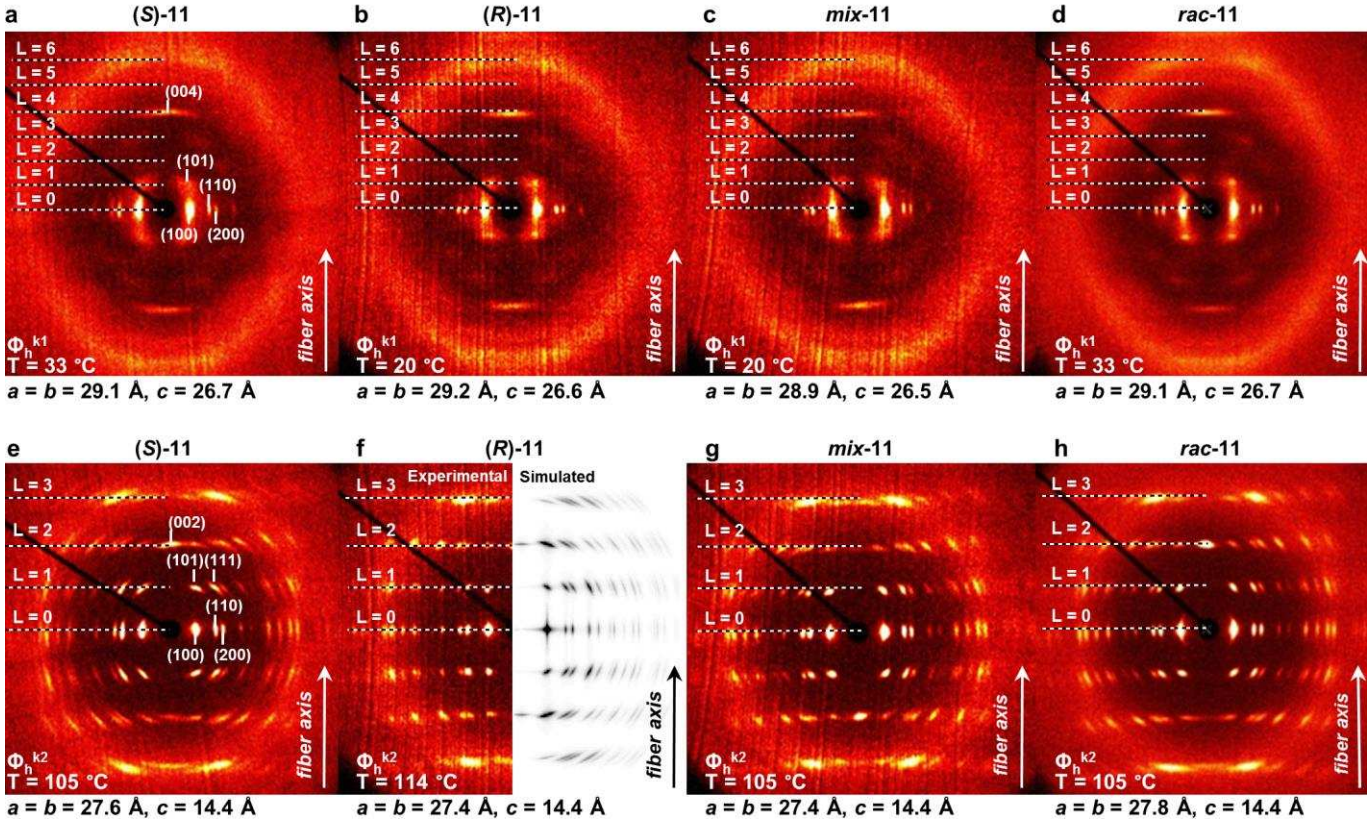

Figure 4. Oriented fiber X-ray diffraction (XRD). XRD patterns collected from oriented fibers of **a**, **e**, **(S)-11**; **b**, **f**, **(R)-11**; **c**, **g**, **mix-11**; and **d**, **h**, **rac-11** in the **a–d**, Φ_h^{k1} and **e–h**, Φ_h^{k2} phases, respectively. **f**, right, Comparison of experimental XRD pattern with XRD pattern simulated from molecular model of **(R)-11** presented in Fig. 5d, f. Fiber axis, temperature, phase, and lattice parameters (a = b = D, where D is the column diameter, Supplementary Table S1) are indicated. Fully indexed patterns for **(R)-11** (**b**, **f**) showing L = 8 and L = 4 layer lines are in Supplementary Fig. S12. The XRD patterns of the Φ_h^{k1} and Φ_h^{k2} phases are, respectively, identical irrespective of the chiral composition of **11**. These patterns demonstrate that homochiral **(S)-** and **(R)-11** and both racemic derivatives, **mix- and rac-11**, self-assemble to give identical supramolecular structure with low order in the Φ_h^{k1} phase and high order in the Φ_h^{k2} phase. The cross-like pattern of diffraction peaks in all diffraction patterns indicates that the assembled structures are helical.

Structural analysis of supramolecular assemblies by X-ray diffraction. X-ray fiber patterns of Φ_h^{k1} of all chiral compositions of **11** were collected from oriented fibers extruded[41] from non-annealed powders (Fig. 4a–d). Annealing for more than 12 days at 23 °C or for shorter times at higher temperatures transformed Φ_h^{k1} into Φ_h^{k2} (Fig. 4e–h, Supplementary Figs. S10–S12). Crystallographic layer lines, L = l, are labelled in Fig. 4 and selected reflections are identified in Fig. 4a, e. Irrespective of the chiral composition and as suggested by ~~the~~ DSC ~~data~~ (Supplementary Fig. S2), Φ_h^{k1} and Φ_h^{k2} are identical in all samples of **11** (Fig. 4). Sharp reflections on layer line L = 0 of Φ_h^{k1} (Fig. 4a–d) indicate well-ordered columns arranged on the projection of the 3D hexagonal lattice along the c-axis (ab-plane of the 3D unit cell, Supplementary Fig. S12). Diffuse streaks extending from the meridian and quadrants demonstrate a helical arrangement of the columns.[13,14,21] The lattice parameters of Φ_h^{k1} and Φ_h^{k2} are listed in Fig. 4 and

Supplementary Table S1. The c-axis length in Φ_h^{k1} is almost double that in Φ_h^{k2} (26.6 Å vs 14.4 Å). Unit cell dimensions and experimental density (1.05 g/cm^3) indicate that eight molecules form the unit cell of Φ_h^{k1} and only four form the unit cell of Φ_h^{k2}. The (008) reflection of Φ_h^{k1} (Supplementary Fig. S12) corresponds to a 3.3 Å π–π stacking distance between successive PBI units. The meridional (004) reflection suggests a 4-fold repeat stacking along the c-axis in Φ_h^{k1}. The presence of the (101) reflection at L = 1 in Φ_h^{k1} suggests a certain degree of intercolumnar crystalline order. However, the lack of other off-meridional reflections indicates that this intercolumnar order is weak and therefore Φ_h^{k1} has only short-range helical order, in line with CD (Fig. 3c) and NMR (Fig. 6 and Supplementary Section S10) experiments. In contrast, Φ_h^{k2} is a highly ordered columnar hexagonal crystal with long range intra- and intercolumnar order, as evidenced by numerous sharp reflections in its XRD pattern (Fig. 4e–h) and solid state NMR analysis (Fig. 6). The absence of (001) coupled with the observation of a nonzero (002) reflection in Φ_h^{k2} indicates that the PBI molecules may be dimerized, as supported by CD and UV-vis experiments (Fig. 2), and that this aggregation consists at least in part of distortions along the c-axis.

The diameter of the Φ_h^{k1} column is only slightly larger than that of the Φ_h^{k2} column (29.2 Å vs 27.4 Å). Modeling shows that a supramolecular column assembled from **11** with alkyl chains extended perpendicular to the column has a maximum diameter of 44 Å (Supplementary Fig. S15b, c). The experimental column diameter (27.4 Å) can only be explained by the model of Φ_h^{k2} from Fig. 5d, f with diameter of 27.7 Å (Supplementary Fig. S15a), in which the alkyl groups are extended parallel to the column axis. Polarized infrared (IR) experiments in aligned films of **rac-11** in the Φ_h^{k2} phase support the arrangement of alkyl chains parallel to the column axis (Supplementary Section S24).

Each unit cell of Φ_h^{k2} contains only one column (Fig. 7b, brown area). Since the unit cell repeats itself three-dimensionally across the entire crystal, this implies that every column in the crystal must be identical with the same helical handedness in order to form a perfect hexagonal crystal.[21] This is true even for **rac-11** and **mix-11**. The Φ_h^{k2} crystal of the racemic compounds show no CD signal in thin film but exhibit signals in micro-spot CD experiments (Fig. 3c and Supplementary Fig. S7). These micro-spot CD data, in combination with changes in contrast in the optical polarized micrographs (Fig. 3d, e) and the identical patterns and Φ_h^{k2} lattice symmetry evidenced by fiber XRD (Fig. 4g, h), provide three complementary techniques that demonstrate that chiral self-sorting or deracemization occurs at the supramolecular level during or after assembly of **mix-11** and **rac-11** to produce hexagonal crystals containing enantiopure domains of single-handed columns. This high order in Φ_h^{k2} is unexpected since only low crystalline order[21] or no crystallization was previously observed in related assemblies comprising single-handed monodomains produced from non-deracemizing racemic building blocks.[32,34]

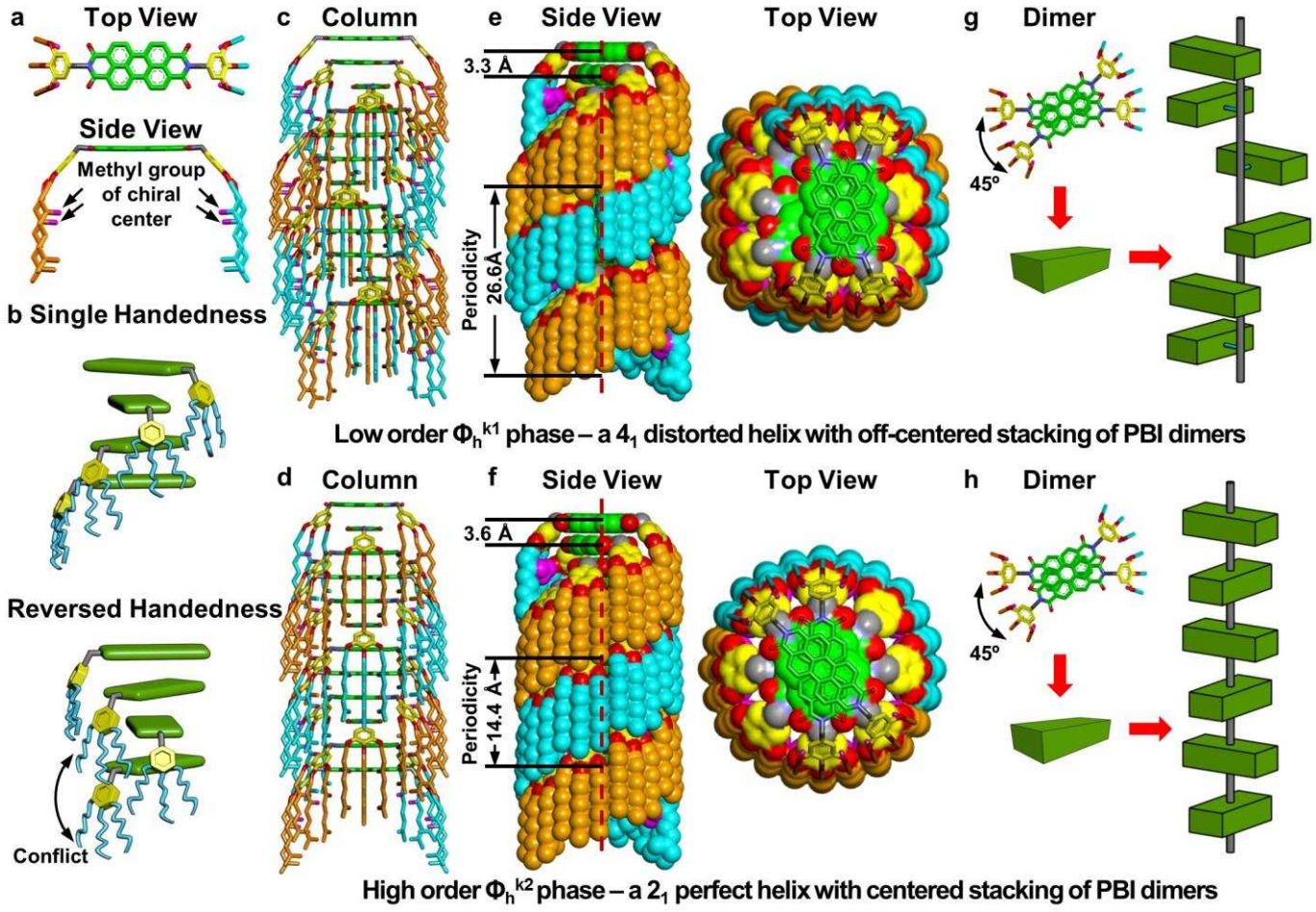

Figure 5. Model of supramolecular packing in the Φ_h^{k1} and Φ_h^{k2} phases. **a**, Single molecular conformation in Φ_h^{k2} of **(R)-11** from top and side views. **b**, Simplified models of four molecules (two dimers) stacked in a column with single handedness (top) and reversed handedness (bottom) showing conflict between periphery alkyl chains. **c**, **d**, Side views of stick column models and **e**, **f**, space filling models for Φ_h^{k1} and Φ_h^{k2}. **g**, **h**, Schematic intracolumnar arrangement of dimers in the two phases. The high steric interaction between alkyl groups upon helix reversal ensures that an assembling column maintains the same helicity along its entire length. Molecules of **11** organize into dimers, which then aggregate to form the supramolecular column in both the Φ_h^{k1} and Φ_h^{k2} phases. The dimers in both phases are identical, but their relative arrangement defines the difference between the two phases: in the low order Φ_h^{k1} phase, the dimers are arranged off-axis, leading to a staggered surface on the exterior of the column; in the high order Φ_h^{k2} phase, the dimers are arranged co-axially generating a smooth column exterior and mediating higher order packing of the supramolecular columns.

Models of supramolecular single-handed helical columns forming the low order Φ_h^{k1} and high order Φ_h^{k2} crystals are shown in Fig. 5. In columns of both phases, two neighboring molecules are stacked and rotated by 45° with respect to each other to form dimers (Fig. 5g, h). In Φ_h^{k2}, the helical axis corresponds to the center of each column, whereas the axis is off-center in the columns comprising Φ_h^{k1}. Consequently, in Φ_h^{k1}, a 4_1-helix with a pitch of 26.6 Å is formed, and in Φ_h^{k2}, a 2_1-helix with a pitch of 14.4 Å is formed.

This structure can also be crystallographically defined as a double helix that is different from that of DNA, whose strands are covalent, while here they are supramolecular (Supplementary Section S19).

The sense of the 45° rotation between neighboring molecules is selected by their chirality. The rotation of racemic dimers is also single-handed but statistically forms racemic crystals with large single-handed domains. The alkyl chains extend parallel to the column axis with the methyl stereocenters pointing into internal gaps defined by the rotation of the supramolecular helical backbone of PBI cores (Fig. 5a–d). This arrangement, demonstrated by the column diameter (Fig. 4 and Supplementary Fig. S15), by the simulation of XRD[21] (Fig. 4f) of the supramolecular model from Fig. 5d, f, by UV analysis in solution (Fig. 2a, bottom) and thin film in $\mathbf{\Phi_h^{k2}}$ (Fig. 3c), and by solid state NMR (Fig. 6), explains the mechanism by which the chirality of mismatched enantiomers or racemic molecules neither affects neighboring columns (Fig. 7~~6~~) nor distorts the highly-ordered hexagonal crystal structure (Fig. 5a, c–f). The length of the alkyl chains matches perfectly with the half-pitch of the helix, thus optimizing organization into helices and providing a principle for the design of additional building blocks following the same self-assembly and crystallization mechanisms.

This model resembles a cogwheel (Fig. 5c–f and Fig. 7), with 24 alkyl chains on the periphery of the column forming teeth. Slight interlocking (0.3 Å) with adjacent single-handed columns reduces the column diameter from a theoretical value of 27.7 Å (Supplementary Fig. S15) to the experimental value of 27.4 Å (Fig. 4e–h) and thus generates the high order observed in the $\mathbf{\Phi_h^{k2}}$ crystal. Theoretical and experimental values for the column diameter in $\mathbf{\Phi_h^{k1}}$ are 28.9 and 29.1 Å, respectively. The diameters of the columns as modeled are supported by X-ray data (Fig. 4 and Supplementary Fig. S15). The helix reversal penalty (1.5 kcal/mol, Supplementary Table S2) is higher than the chiral mismatch penalty (0.6 kcal/mol, Supplementary Table S2), that is, the energetic penalty for a chiral monomer to add to a helix of its non-preferred handedness (compare bottom and top, Fig. 5b). This provides the mechanism by which a monomer with non-preferred chirality or even mixed chiral character is incorporated in a single-handed helix. The handedness of all dimers is the same within a column (Fig. 5b), and therefore crystals of racemic compounds have a racemic mixture of left- and right-handed columns, segregated into crystalline domains of single handedness columns (Figs 3c and 7). This allows the generation of columns with indistinguishable cogwheel shapes from non-deracemizing **rac-11** and the formation of hexagonal crystals with as high a degree of order as those formed from enantiomerically pure compounds (Fig. 7).

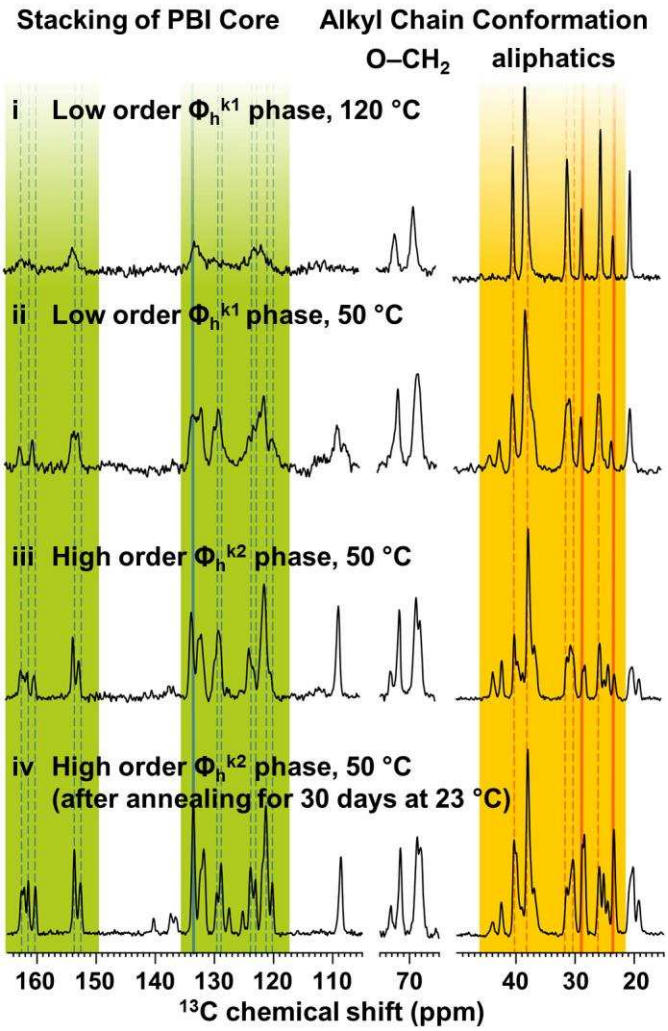

Figure 6. ^{13}C Cross-Polarization Magic Angle Spinning (CP-MAS) solid state NMR studies. ^{13}C CP-MAS solid state NMR spectra of **rac-11** in **i**, low order $\mathbf{\Phi_h^{k1}}$ phase at 120 °C; **ii**, low order $\mathbf{\Phi_h^{k1}}$ phase at 50 °C; **iii**, high order $\mathbf{\Phi_h^{k2}}$ phase at 50 °C; **iv**, high order $\mathbf{\Phi_h^{k2}}$ phase at 50 °C after annealing the sample for 30 days at 23 °C. Green highlighted areas correspond to signals arising from the PBI core. Yellow highlighted areas correspond to signals arising from the aliphatic chains at the periphery of the structure. The broad aromatic peaks in the low order $\mathbf{\Phi_h^{k1}}$ phase at high temperature sharpen significantly upon cooling the $\mathbf{\Phi_h^{k1}}$ phase, in the $\mathbf{\Phi_h^{k2}}$ phase and, unexpectedly, by allowing the $\mathbf{\Phi_h^{k2}}$ phase to anneal at 23 °C for 30 days. This indicates that the optimal molecular packing is very well defined for **rac-11**, and that even in the high order phase, sufficient molecular fluctuations are present in order to refine and improve the supramolecular structure of the crystal on very long time scales.

Solid state NMR experiments. Solid state NMR experiments of assemblies of **11** support the structure determined by XRD (Fig. 6 and Supplementary Figs S4 and S5). ^{13}C Cross-Polarization (CP) MAS spectra of $\mathbf{\Phi_h^{k1}}$ of **rac-11** exhibit broadening of the aromatic signals on cooling to 120 °C and 50 °C due to molecular motions mediated by the irregular packing of the PBI core (Fig. 6i, ii). In contrast, well resolved signals are obtained in $\mathbf{\Phi_h^{k2}}$ at 50 °C, indicating a regular packing of the aromatic part of the PBI (Fig. 6iii). The –CH_2O– and aliphatic chain signals follow the same trend with respect to order, indicating a liquid-like molecular motion in $\mathbf{\Phi_h^{k1}}$ and almost perfect conformational order in $\mathbf{\Phi_h^{k2}}$ that is unexpected for the short

and branched dimethyloctyl chains.[50] Repeating the CP-MAS experiment with **rac-11** after extended annealing at ambient temperature (30 days, 23 °C) improves the spectral resolution due to substantially improved packing in the aromatic and aliphatic side chains (Fig. 6iv). This indicates that very well defined packing of the alkyl groups in the highly ordered $\mathbf{\Phi_h^{k2}}$ phase of **rac-11** is achieved due to sufficient molecular fluctuations that refine and improve the molecular structure of the periodic array on very long time scales. 2D $^{13}C\{^1H\}$ heteronuclear Lee-Goldburg Cross-Polarization (LGCP) correlation experiments and additional CP-MAS experiments with **(R)-11** and **rac-11** provide further details on these observations (Supplementary Section S10).

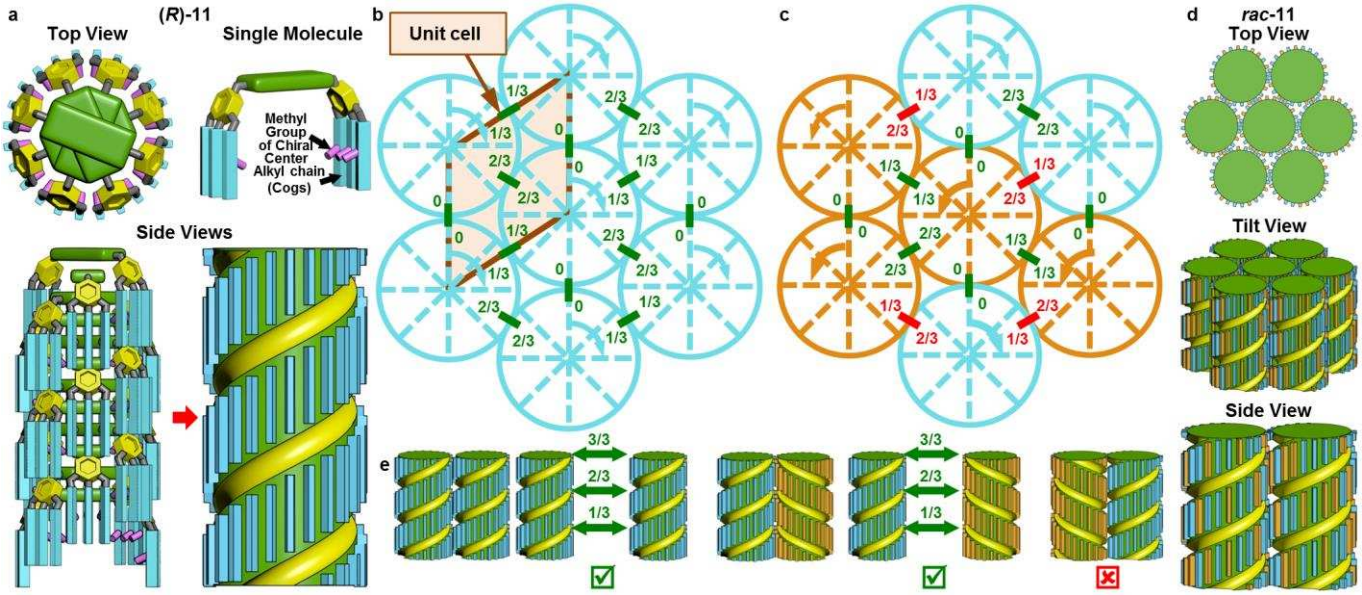

Figure 7. **Cogwheel model of self-assembly and its role in generating microdomains of single-handed supramolecular columns. a**, Schematic representation of a right-handed column produced by **(R)-11** from top and side views. The supramolecular column (left) can be considered as a cogwheel (right). Conformation of a single molecule within the column is also shown. **b**, **c**, Schematic packing of helical columns with **b**, single handedness and **c**, mixture of two handednesses (Supplementary Section S21). Right- and left-handed helical columns are denoted in blue and orange, respectively. The relative heights of the grooves at the interfaces between adjacent columns are indicated as a fraction of column length (0, 1/3, 2/3). Grooves with matching and mismatching interfacial heights are presented in green and red, respectively. In **b**, the unit cell of $\mathbf{\Phi_h^{k2}}$ lattice containing a single helical column is marked in brown. **d**, Columns of **rac-11** packed in a right-handed crystal domain from top and side views. **e**, Schematic representations of the alignment of the grooves of neighboring columns: (left) matching between columns of the same handedness; (center) matching between columns of different handedness; (right) mismatching between columns of different handedness. In **d**–**e**, blue and orange teeth represent chiral alkyl chains with different chiralities.

The proposed cogwheel model (Fig. 7a) requires the helical packing of molecules with alkyl chains parallel to the column axis and methyl groups pointed toward the center of the column. Within each supramolecular column, the teeth (alkyl chains, Fig. 7a, bottom right) are hydrophobic while the grooves are more polar due to the ether linkages between the alkyl chains and aromatic rings. During self-assembly, the columns

seek to maximize the intercolumnar electrostatic and hydrophobic interactions by vertically aligning the alkyl chains at the interface between columns. Only packing with the same handedness columns ~~can~~ simultaneously optimizes the interactions with all neighbors ~~at the same time~~ by positioning the grooves of neighboring columns at the same height (Fig. 7b, c, e and Supplementary Information). The grooves of columns of the same handedness (Fig. 7e, left) will always align in all directions. In contrast, the grooves of columns of different handedness will align in some instances (Fig. 7e, center) but not in others (Fig. 7e, right; see also Fig. 7c). It is a requirement of $\mathbf{\Phi_h^{k2}}$ that all columns have the same handedness, as there is only one column in the crystallographic unit cell (Fig. 7b). Aligning the grooves and teeth of adjacent columns provide a mechanism through which only columns with the same handedness pack together to form highly ordered crystals, even in fully racemized~~,~~ **rac-11** (Fig. 7d).

Conclusion

The cogwheel columnar model from Figs 5 and 7 and its role in enabling deracemization in supramolecular assemblies is demonstrated herein by three key complementary techniques: variable temperature XRD of oriented fibers (Fig. 4 and Supplementary Figs S10–S12 and S16), microspot CD of thin films (Fig. 3c and Supplementary Figs S7 and S8) and optical polarized microscopy (Fig. 3d, e), as well as a diversity of other supporting techniques including solid state NMR (Fig. 6 and Supplementary Section S10), solution CD (Fig. 2), DSC (Supplementary Fig. S2), molecular modeling (Supplementary Fig. S15), IR (Supplementary Fig. S17) and UV analysis (Supplementary Fig. S4). This cogwheel model provides a mechanism for perfect packing of single-handed columns irrespective of the chirality of their molecular building blocks (Fig. 7b), as well as near-perfect packing for helical columns with different handednesses (Fig. 7d). We anticipate that the principle of matching the helical half-pitch with the length of the side chains will give access to extended libraries of compounds with similar helical structures. This packing mechanism yields a higher level of hexagonal crystal order in the assemblies of homochiral, racemic, and irreversibly racemized building blocks than any homochiral biological or non-biological single or double helix. The findings reported here challenge the established requirement that highly ordered crystalline systems are achievable only with enantiopure building blocks, and hence provide new access to high order assemblies of chiral PBIs, which have higher charge carrier mobility than achiral counterparts.[35] We therefore envisage that the cogwheel mechanism of self-assembly and self-organization described here will find practical applications in the design of functions in complex materials.

Methods

Synthesis, materials, characterization data and methods for MALDI-TOF, micro-spot CD, POM and density measurements are described in Supplementary Section S2.

Differential scanning calorimetry (DSC). Thermal transitions were determined on a TA Instruments Q100 differential scanning calorimeter equipped with a refrigerated cooling system with 10 °C/min and 1 °C/min heating and cooling rates. Indium was used as a calibration standard. The transition temperatures were calculated as the maxima and minima of their endothermic and exothermic peaks. An Olympus BX51 optical microscope (100× magnification) equipped with a Mettler FP82HT hot stage and a Mettler Toledo FP90 Central Processor was used to verify thermal transitions.

Circular dichroism (CD) spectroscopy in solution. Circular dichroism and UV-vis spectroscopy measurements were carried out on a Jasco J-720 Spectropolarimeter. The temperature was controlled by a Peltier temperature controller (Jasco PTC-423). Methylcyclohexane, cyclohexane (both 99%, spectrophotometric grade, Aldrich) and 1-butanol (99.5%, spectrophotometric grade, Aldrich) were used as solvents. Solution spectra were recorded in 10-mm quartz cuvettes stirred at 1000 rpm with a small magnetic stirring bar, and corrected by subtracting the spectrum of the pure solvent at the same temperature. A scan rate of 100 nm/min with a response time of 1 s and a bandwidth of 1 nm was used to measure the CD spectra, which were recorded in low sensitivity mode between 800 and 200 nm (3 accumulations). Further details are provided in Supplementary Section S2.3.

CD spectroscopy in thin film. Thin film CD/UV experiments were conducted as follows. A 2% w/v solution of **11** in n-butanol/methylcyclohexane (85:15 v/v) was prepared by heating 2 mg of sample in 100 μL of solvent until dissolved. The hot solution was spin-coated on a round quartz plate (22 mm diameter) at 2500 rpm for 6 s and 7000 rpm for 30 s, using a Chemat Technology Spin Coater KW-4A. The thin film was then annealed at 110 °C for 3 h and cooled to room temperature, whereupon measurements were recorded. CD/UV spectra of thin films were recorded using the same parameters as those used for solution experiments, and the spectra were corrected by subtracting spectra of the quartz plate recorded before spin-coating. The presence of linear dichroism was negated by recording CD spectra of the thin film at various rotations perpendicular to the beam and ensuring that the CD spectra was the same, irrespective of rotation.

X-ray diffraction (XRD). X-ray diffraction measurements were performed using Cu-$K_{\alpha 1}$ radiation (λ = 1.542 Å) on a Bruker-Nonius FR-591 rotating anode X-ray source equipped with a 0.2 × 0.2 mm^2

filament and operated at 3.4 kW. The Cu radiation beam was collimated and focused by a single bent mirror and sagittally focused through a Si(111) monochromator, generating a 0.3 × 0.4 mm^2 spot on a Bruker-AXS Hi-Star multiwire area detector. To minimize attenuation and background scattering, an integral vacuum was maintained along the length of the flight tube and within the sample chamber. Samples were held in quartz capillaries (0.7–1.0 mm in diameter), mounted in a temperature-controlled oven (temperature precision: ±0.1 °C, temperature range from –120 °C to 270 °C). Further details are provided in Supplementary Section S2.5.

Preparation of aligned fibers for XRD. Aligned samples for fiber XRD experiments were prepared using a custom-made extrusion device.[41] The powdered sample (~10 mg) was placed inside the extrusion device and the fiber was extruded in the as prepared state ($\mathbf{\Phi_h^{k1}}$ phase) at room temperature without any heat treatment. Typically, the aligned fiber samples have a thickness of 0.3–0.7 mm and a length of 3–7 mm. All XRD measurements were done with the aligned sample axis perpendicular to the beam direction.

Solid state NMR spectroscopy. Variable temperature $^{13}C\{^1H\}$ Cross-Polarization-Magic Angle Spinning (CP-MAS) NMR spectra (Fig. 6) were recorded with a Bruker Avance III console operating at 700.23 MHz ^1H Larmor frequency (176.1 MHz ^{13}C Larmor frequency) using a commercial double resonance probe supporting zirconia rotors with 2.5mm outer diameter. Measurements were performed at 25 kHz MAS spinning frequency using a CP contact time of 1 ms. An rf nutation frequency of 100 kHz was used on both the ^1H and ^{13}C channels, as well as for ^1H heteronuclear decoupling during acquisition using the SPINAL64 scheme. The given temperatures have been corrected for known deviations due to frictional heating under fast spinning conditions based on the temperature dependent chemical shift of lead nitrate. In order to compare the temperature dependence of the CP-MAS signal intensities, spectra with 5120 transients and identical experimental parameters were recorded in the temperature range from 40 to 100 °C. 2D $^{13}C\{^1H\}$ heteronuclear Lee-Goldburg Cross-Polarization (LGCP) correlation experiments (Supplementary Fig. S4) were recorded at 18 kHz MAS and 850 MHz ^1H Larmor frequency using an LGCP contact time of 0.2 ms and 102 kHz FSLG multi pulse decoupling for line narrowing in the ^1H dimension.

References

1. Frank, P., Bonner, W. A. & Zare, R. N. in Chemistry for the 21st Century (eds Keinan, E. & Schechter, I.) 175–208 (Wiley-VCH Verlag GmbH, Weinheim, Germany, 2000).

2. Lehn, J.-M. From supramolecular chemistry towards constitutional dynamic chemistry and adaptive chemistry. Chem. Soc. Rev. **36,** 151–160 (2007).

3. Hein, J. E., Gherase, D. & Blackmond, D. G. Chemical and physical models for the emergence of biological homochirality. Top Curr. Chem. **333,** 83–108 (2013).

4. Rowan, A. E. & Nolte, R. J. M. Helical molecular programming. Angew. Chem. Int. Ed. **37,** 63–68 (1998).

5. Weissbuch, I. & Lahav, M. Crystalline architectures as templates of relevance to the origins of homochirality. Chem. Rev. **111,** 3236–3267 (2011).

6. Pauling, L., Corey, R. B. & Banson, H. R. The structure of proteins: two hydrogen-bonded helical configurations of their polypeptide chain. Proc. Natl. Acad. Sci. USA **3**7, 205–211 (1951).

7. Sarko, A. & Marchessault, R. H. The crystal structure of amylose triacetate. A non-integral helix. Science **154**, 1658–1659 (1966).

8. Natta, G. in Nobel Lectures in Chemistry 1963–1970, 27–60 (World Scientific Publishing Co., Singapore, 1999).

9. Natta, G. et al. Crystalline high polymers of α-olefins. J. Am. Chem. Soc. **77**, 1708–1710 (1955).

10. Iijima, S. Helical microtubules of graphitic carbon. Nature **354,** 56–58 (1991).

11. Saito, R., Fujita, H., Dresselhaus, G. & Dresselhaus, M. S. Electronic structure of chiral carbon tubules. Appl. Phys. Lett. **60**, 2204–2206 (1992).

12. Ebbesen, T. W. et al. Electrical conductivity of individual carbon nanotubes. Nature **382**, 54–56 (1996).

13. Watson, J. D. & Crick, F. H. C. Molecular structure of nucleic acids: a structure for deoxyribose nucleic acid. Nature **171,** 737–738 (1953).

14. Franklin, R. E. & Gosling, R. G. Molecular configuration in sodium thymonucleate. Nature **171,** 740–741 (1953).

15. Klug, A. The discovery of the DNA double helix. J. Mol. Biol. **335,** 3–26 (2004).

16. Pertuz, M. F. in Nobel Lectures, Chemistry 1942–1962 (Elsevier Publishing Company, Amsterdam, 1964).

17. Natta, G. & Corradini, P. The structure of crystalline 1,2-polybutadiene and of other syndiotactic polymers. J. Polym. Sci. **20**, 251–266 (1956).

18. Pasteur, L. On the relations that can exist between crystalline form, and chemical composition, and the sense of rotary polarization. Ann. Chim. Phys. **24,** 442–459 (1848).

19. Azeroual, S. et al. Mirror symmetry breaking and chiral amplification in foldamer-based supramolecular helical aggregates. Chem. Commun. **48,** 2292–2294 (2012).

20. Sisco, S. W. & Moore, J. S. Homochiral self-sorting of BINOL macrocycles. Chem. Sci. **5,** 81–85 (2014).

21. Roche, C. et al. Homochiral columns constructed by chiral self-sorting during supramolecular helical organization of hat-shaped molecules. J. Am. Chem. Soc. **136,** 7169–7185 (2014).

22. González-Campo, A. & Amabilino, D. Biomolecules at interfaces: chiral, naturally. Top Curr. Chem. **333,** 109–156 (2013).

23. Fletcher, S. P., Jagt, R. B. C. & Feringa, B. L. An astrophysically-relevant mechanism for amino acid enantiomer enrichment. Chem. Commun. **43,** 2578–2580 (2007).

24. Sato, K., Itoh, Y. & Aida, T. Homochiral supramolecular polymerization of bowl-shaped chiral macrocycles in solution. Chem. Sci. **5,** 136–140 (2014).

25. Safont-Sempere, M. M., Fernández, G. & Würthner, F. Self-sorting phenomena in complex supramolecular systems. Chem. Rev. **111,** 5784–5814 (2011).

26. Link, D. R. et al. Spontaneous formation of macroscopic chiral domains in a fluid smectic phase of achiral molecules. Science **278**, 1924–1927 (1997).

27. Nagayama, H. et al. Spontaneous deracemization of disc-like molecules in the columnar phase. Angew. Chem. Int. Ed. **49**, 445–448 (2010).

28. Jeong, H. S. et al. Spontaneous chirality induction and enantiomer separation in liquid crystals composed of achiral rod-shaped 4-arylbenzoate esters. J. Am. Chem. Soc. **131**, 15055–15060 (2009).

29. Klug, A. From macromolecules to biological assemblies (Nobel Lecture). Angew. Chem. Int. Ed. Engl. **22**, 565–582 (1983).

30. Klug, A. The tobacco mosaic virus particle: structure and assembly. Phil. Trans. R. Soc. London, Ser. B **354**, 531–535 (1999).

31. Percec, V. et al. Self-assembly of amphiphilic dendritic dipeptides into helical pores. Nature **430,** 764–768 (2004).

32. Rosen, B. M. et al. Programming the supramolecular helical polymerization of dendritic dipeptides via the stereochemical information of the dipeptide. J. Am. Chem. Soc. **133,** 5135–5151 (2011).

33. Percec, V. & Leowanawat, P. Why are biological systems homochiral? Isr. J. Chem. **51**, 1107–1117 (2011).

34. Rosen, B. M., Roche, C. & Percec, V. Self-assembly of dendritic dipeptides as a model of chiral selection in primitive biological systems. Top Curr. Chem. **333,** 213–254 (2013).

35. Dehm, V. et al. Helical growth of semiconducting columnar dye assemblies based on chiral perylene bisimides. Org. Lett. **9,** 1085–1088 (2007).

36. Sanchez-Valencia, J. R. et al. Controlled synthesis of single-chirality carbon nanotubes. Nature **512,** 61–64 (2014).

37. Pokroy, B., Kang, S. H., Mahadevan, L. & Aizenberg, J. Self-organization of a mesoscale bristle into ordered, hierarchical helical assemblies. Science **323,** 237–240 (2009).

38. Percec, V. et al. Controlling polymer shape through the self-assembly of dendritic side-groups. Nature **391,** 161–164 (1998).

39. Percec, V. et al. Self-organization of supramolecular helical dendrimers into complex electronic materials. Nature **419,** 384–387 (2002).

40. Arias, S., Freire, F., Quiñoá, E. & Riguera, R. Nanospheres, nanotubes, toroids, and gels with controlled macroscopic chirality. Angew. Chem. Int. Ed. **53,** 13720–13724 (2014).

41. Peterca, M. et al. Molecular structure of helical supramolecular dendrimers. J. Am. Chem. Soc. **130,** 14840–14852 (2008).

42. Percec, V. et al. Transformation from kinetically into thermodynamically controlled self-organization of complex helical columns with 3D periodicity assembled from dendronized perylene bisimides. J. Am. Chem. Soc. **135,** 4129–4148 (2013).

43. Jonkheijm, P., van der Schoot, P., Schenning, A. P. H. J. & Meijer, E. W. Probing the solvent-assisted nucleation pathway in chemical self-assembly. Science **313,** 80–83 (2006).

44. Percec, V., Ungar, G. & Peterca, M. Self-assembly in action. Science **313,** 55–56 (2006).

45. Smulders, M. M. J. et al. How to distinguish isodesmic from cooperative supramolecular polymerisation. Chem. Eur. J. **16,** 362–367 (2010).

46. Van Gestel, J. Amplification of chirality in helical supramolecular polymers: the majority-rules principle. Macromolecules **37,** 3894–3898 (2004).

47. Green, M. M. et al. Majority rules in the copolymerization of mirror image isomers. J. Am. Chem. Soc. **117,** 4181–4182 (1995).

48. Van Gestel, J., Palmans, A. R. A., Titulaer, B., Vekemans, J. A. J. M. & Meijer, E. W. "Majority-rules" operative in chiral columnar stacks of C_3-symmetrical molecules. J. Am. Chem. Soc. **127,** 5490–5494 (2005).

49. Jin, W. et al. Self-assembled graphitic nanotubes with one-handed helical arrays of a chiral amphiphilic molecular graphene. Proc. Natl Acad. Sci. USA **102,** 10801–10806 (2005).

50. Ungar, G. & Masic, N. Order in the rotator phase of n-alkanes. J. Phys. Chem. **89,** 1036–1042 (1985).

Acknowledgements Financial support by the National Science Foundation (DMR-1066116, DMR-1120901 and OISE-1243313), the Humboldt Foundation, and the P. Roy Vagelos Chair at Penn (all to V.P.) is gratefully acknowledged. G.U. and X.Z. acknowledge support from the joint NSF-EPSRC PIRE project "RENEW" (EPSRC grant EP-K034308). B.E.P. thanks the Howard Hughes Medical Institute for an International Student Research Fellowship. We thank Ihtesham ur Rehman (University of Sheffield, UK) for recording polarized IR spectra.

Author contributions C.R., P.L., B.E.P. and D.A.W. synthesized and characterized compounds; C.R., B.E.P., D.A.W. and M.E.P. performed solution state CD and UV-vis analysis; F.A. performed micro-spot CD analysis; H.-J.S., M.P. and B.E.P. collected and processed X-ray diffraction data; X.Z., H.-J.S., P.A.H. and G.U. generated the molecular model; H.-J.S. and B.E.P. simulated X-ray data; R.G. and H.W.S. performed solid state NMR analysis; V.P. designed the study; V.P., B.E.P., C.R., and H.-J.S. analyzed data and prepared the manuscript. All authors discussed the results and commented on the manuscript.

Additional information Supplementary information and chemical compound information are available in the online version of the paper. Reprints and permissions information is available at www.nature.com/reprints. Correspondence and requests for materials should be addressed to V.P.

Competing financial interests The authors declare no competing financial interests.